



HAL
open science

Hybridization of volumetric and surface models for the computation of the T/R EC probe response due to a thin opening flaw

Léa Maurice, Denis Prémel, József Pávó, Dominique Lesselier, Alain Nicolas

► **To cite this version:**

Léa Maurice, Denis Prémel, József Pávó, Dominique Lesselier, Alain Nicolas. Hybridization of volumetric and surface models for the computation of the T/R EC probe response due to a thin opening flaw. *COMPEL: The International Journal for Computation and Mathematics in Electrical and Electronic Engineering*, 2008, 27 (1), pp.298 - 306. 10.1108/03321640810836852 . hal-00395401

HAL Id: hal-00395401

<https://hal.science/hal-00395401>

Submitted on 6 Feb 2024

HAL is a multi-disciplinary open access archive for the deposit and dissemination of scientific research documents, whether they are published or not. The documents may come from teaching and research institutions in France or abroad, or from public or private research centers.

L'archive ouverte pluridisciplinaire **HAL**, est destinée au dépôt et à la diffusion de documents scientifiques de niveau recherche, publiés ou non, émanant des établissements d'enseignement et de recherche français ou étrangers, des laboratoires publics ou privés.

Hybridization of volumetric and surface models for the computation of the T/R EC probe response due to a thin opening flaw

L. Maurice¹, D. Prémel¹, J. Pávó², D. Lesselier³, A. Nicolas⁴.

¹ C.E.A Saclay, SYSSC, Bât. 611, 91191 Gif-sur-Yvette Cedex, France

² Budapest University of Technology and Economics, H-1521 Budapest, Hungary

³ DRE - L2S (CNRS - Supélec - UPS 11), 91192 Gif-sur-Yvette Cedex, France

⁴ ECL CEGELY, 36 avenue Guy de Collongue, Bât. H9, 69134 Ecully, France.

Abstract — This paper concerns the development of simulation tools dedicated to Eddy Current Non Destructive Testing (ECNDT) on planar structures implying planar defects. Two integral approaches using the Green dyadic formalism are considered. The Surface Integral Model (SIM) is dedicated to ideal cracks, whereas the Volume Integral Method (VIM) is adapted to general volumetric defects. We observed that SIM provides satisfactory results, except in some critical Transmitting / Receiving (T/R) configurations. This led us to propose a hybrid method based on the combination of the two previous ones.

I. INTRODUCTION

Eddy Current (EC) interactions with planar defects, *i.e.* defects which have an opening width much smaller than the length of the flaw, have been studied by many authors in the last two decades. A useful approach consists in an idealization of such defects through the definition of an ideal thin crack: Assuming that the thickness tends toward zero, the thin crack acts as an impenetrable barrier to the electric current [1]. In the case of a transverse planar flaw, the spatial variable x along the thickness of the flaw disappears, and the flaw is represented by a current surface dipole density, referred to as $p(y, z)$, which is a scalar quantity depending on two spatial variables corresponding to the dimensions of the surface of the ideal flaw. The surface dipole density is solution of an integral equation on the surface of the crack, which involves an hypersingular kernel when it is evaluated in the spatial domain [2, 3]. In an alternative way the kernel can be evaluated in the spectral domain [4], and the use of a global approximation of $p(y, z)$ may overcome some numerical difficulties coming from specific boundary conditions to be satisfied by $p(y, z)$ [5]. This numerical approach leads to the implementation of a fast numerical model [6] which can advantageously be integrated in an iterative procedure for probe design or for performing some parametric studies [7].

While testing this model on some T/R configurations, we nevertheless noticed unsuitable results. This led us to compare them to results yielded by the VIM, whose efficiency had already been demonstrated for a great number of NDT configurations [8, 9].

In a first part, this paper gives a review of SIM and VIM, and a third model is proposed, set up thanks to a combination of SIM and VIM. In a second part, we carry out experiments on T/R probes to evaluate the respective performances of each model, regarding the accuracy of results as well as the computational time and the computational load required.

II. DESCRIPTION OF THE MODELS

Let us consider a conducting non-magnetic slab of conductivity σ_0 . It is tested with an air-core probe functioning either in absolute or in Transmitting / Receiving (T/R) mode, and featuring respectively one or several coils. We operate in a time-harmonic regime, with an excitation assumed to vary

in time as the real part of $\exp(-i\omega t)$. The driving current in the transmitting coil (respectively in the receiving coil) has a magnitude of I^T (respectively I^R) and ω stands for the angular frequency.

A. Surface Integral Model (SIM)

This model is based on the idealization of the perfectly non-conducting planar flaw, as defined in the introduction. The ideal crack is represented by an equivalent surface distribution : the dipole surface density $p(\mathbf{r}_s)$ defined by [1]:

$$\mathbf{E}_t^+(\mathbf{r}_s) - \mathbf{E}_t^-(\mathbf{r}_s) = -\frac{1}{\sigma_0} \nabla_t p(\mathbf{r}_s) \quad (1)$$

where $\mathbf{r}_s = (y, z)$ is the variable describing the surface of the flaw, $\mathbf{E}_t^+(\mathbf{r}_s)$ and $\mathbf{E}_t^-(\mathbf{r}_s)$ are the tangential components of $\mathbf{E}(\mathbf{r}_s)$, the electric field in the vicinity of the flaw, on both sides of the flaw. ∇_t is the differential operator once the normal derivative is removed.

Denoting \mathbf{E}^P the primary field due to the emitting part of the probe, S_f the surface of the flaw, \mathbf{n} the unit vector normal to S_f , μ_0 the permeability of the vacuum, the dipole surface density is determined by solving:

$$\mathbf{E}^P(\mathbf{r}_0) \cdot \mathbf{n} = - \lim_{\mathbf{r}_s \rightarrow \mathbf{r}_0 \in S_f} i\omega\mu_0 \int_{S_f} G^{\text{nn}}(\mathbf{r}_s|\mathbf{r}'_s) p(\mathbf{r}'_s) d\mathbf{r}'_s \quad (2)$$

with $G^{\text{nn}}(\mathbf{r}_s|\mathbf{r}'_s) = \mathbf{n} \cdot \overline{\mathbf{G}}(\mathbf{r}_s|\mathbf{r}'_s) \cdot \mathbf{n}$, and $\overline{\mathbf{G}}(\mathbf{r}_s, \mathbf{r}'_s)$ is the electric-electric dyadic Green's function [10].

The probe response is given by [1]:

$$I^T \cdot I^R \Delta Z = - \int_{S_f} \mathbf{E}^R(\mathbf{r}_s) \cdot \mathbf{n} p(\mathbf{r}_s) d\mathbf{r}_s \quad (3)$$

where \mathbf{E}^R is the electric field which would be due to the receiving coil assumed to operate in the source mode. The transmitting and the receiving coils are identical in the case of an absolute probe, so $I^T = I^R$ and $\mathbf{E}^R = \mathbf{E}^P$, thus retrieving the usual formula of impedance [1]. This model has been experimentally validated [6], and a global decomposition of $p(\mathbf{r}_s)$ is used [11] for the case of rectangularly-shaped flaws, written:

$$p(y, z) = \sum_{m_y=1}^{M_y} \sum_{m_z=1}^{M_z} p^{m_y, m_z} f_y^{m_y}(y) f_z^{m_z}(z) \quad (4)$$

The approximating functions are defined on the whole surface of the crack, and their explicit formulation, *e.g.*, for a surface breaking flaw, is:

$$f_y^{m_y}(y) = \sqrt{\frac{2}{b}} \cdot \sin\left(\frac{m_y}{b} \pi \left(y + \frac{b}{2}\right)\right)$$

$$f_z^{m_z}(z) = \sqrt{\frac{2}{a}} \cdot \cos\left(\frac{2m_z-1}{2a} \pi z\right)$$

where $f_y^{m_y}$ and $f_z^{m_z}$ are respectively the m_y^{th} and m_z^{th} mode functions in the y and z direction. b and a respectively stand for the length of the flaw along the y dimension, and the depth of the flaw, along the z dimension. Three other definitions of the $f_z^{m_z}$ functions are obtained by applying the boundary conditions on the Fourier modes for the three other types of defects, namely: flaws opening at the bottom of the plate, embedded cracks, and through-wall cracks [11].

The main advantage of this global approximation is that it enables to take into account the boundary conditions on $p(\mathbf{r}_s)$, namely [5]:

$$\begin{cases} p = 0 & \text{on embedded edges} \\ \frac{\partial p}{\partial z} = 0 & \text{on surface-breaking edges} \end{cases} \quad (5)$$

This ensures a better accuracy compared to the approximation based on local functions [11]. Equation (3) reveals on the one hand that SIM does not take into account all the components of the electric primary field $\mathbf{E}^P(\mathbf{r}_s)$, but only the normal one. On the other hand, it should be pointed out that the actual volume of the defect is always enforced to zero. These features could be reasons why we sometimes notice a lack of accuracy on the results, as it is illustrated in the following. Now we propose to examine the behaviour of the VIM model in the case of thin cracks.

B. Volumetric Integral Model (VIM)

VIM is a non-dedicated model that provides probe responses in case of general 3D defects, characterized by a local conductivity of $\sigma(\mathbf{r})$, with $\mathbf{r} = (x, y, z)$ denoting henceforth the usual 3-D variable. The presence of the defect is taken into account by considering a volumetric dipole distribution \mathbf{P} given by :

$$\mathbf{P}(\mathbf{r}) = (\sigma(\mathbf{r}) - \sigma_0)\mathbf{E}(\mathbf{r}) \quad (6)$$

$\mathbf{E}(\mathbf{r})$ is determined by solving the following state equation, where V_d is the volume of the flaw:

$$\mathbf{E}(\mathbf{r}) = \mathbf{E}^P(\mathbf{r}) + i\omega\mu_0 \int_{V_d} \overline{\mathbf{G}}(\mathbf{r}, \mathbf{r}')\mathbf{P}(\mathbf{r}')d\mathbf{r}' \quad (7)$$

According to the reciprocity theorem [12], the probe response is given by the following equation:

$$I^T \cdot I^R \Delta Z = - \int_{V_d} \mathbf{E}^R(\mathbf{r}) \cdot \mathbf{P}(\mathbf{r}) d\mathbf{r} \quad (8)$$

with the same remark as previously for the case of an absolute probe.

Different simulation tools based on this numerical approach are integrated in the CIVA platform [13].

In the case of thin opening flaws, the high variations of the tangential component of the electric field on both sides of the flaw require to refine the mesh in the thickness of the flaw. This leads to an increased computational time and a large allocation of memory to reach satisfactory accuracy in some cases.

We propose to build up a hybrid model, taking benefit from the advantages of each model.

C. Hybrid Model (HybM)

The planar defect is of zero conductivity, and described by a fictitious volumetric current density $\mathbf{P}(\mathbf{r})$ which satisfies:

$$\mathbf{P}(\mathbf{r}) = -\sigma_0 \cdot \mathbf{E}^T(\mathbf{r}) \quad (9)$$

where $\mathbf{r} = (x, y, z)$, $\mathbf{E}^T(\mathbf{r})$ is the total electric field due to the interaction between the primary field $\mathbf{E}^P(\mathbf{r})$ and the flaw. $\mathbf{E}^T(\mathbf{r})$ can be approximated by the electric field of the corresponding ideal thin crack given by [1]:

$$\mathbf{E}^T(\mathbf{r}) = \mathbf{E}^P(\mathbf{r}) + i\omega\mu_0 \int_{S_f} \overline{\mathbf{G}}(\mathbf{r}, \mathbf{r}'_s) \cdot \mathbf{n} p(\mathbf{r}'_s) d\mathbf{r}'_s \quad (10)$$

The probe response is then given by:

$$I^T \cdot I^R \Delta Z = \sigma_0 \int_{V_d} \mathbf{E}^R(\mathbf{r}) \cdot \mathbf{E}^T(\mathbf{r}) d\mathbf{r} \quad (11)$$

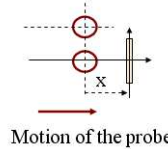
with again simplifications in the case of an absolute probe. In equation (11), the normal and tangential components of the primary field are taken into account, on the whole volume of the defect V_d . Moreover, equation (10) involves the scalar dipole density $p(\mathbf{r}_s)$, fast yielded by SIM, and only three of the nine components of the $\overline{\mathbf{G}}(\mathbf{r}, \mathbf{r}')$ dyad are needed. It should also be stressed that, in contrast with VIM, this method does not require any matrix inversion. All these features makes HybM in principle faster than VIM, and more accurate than SIM. A set of validations, presented in the next section, has been carried out in order to assess HybM performances.

III. VALIDATIONS

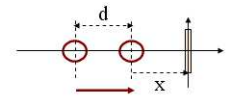
A. Comparison to experimental data on a first arrangement

We consider a 1.55-mm-thick slab, made of Inconel 600 of conductivity $\sigma_0 = 1.02$ MS/m. We study the response of two surface-breaking flaws, characterized both by a length of 7 mm, and a width of 0.1 mm. They differ in depth: The notch denoted by "N1" has a depth of 1.24 mm, *i.e.* 80% of the whole thickness of the slab, whereas "N2" denotes a 60% depth notch (0.92 mm).

The probe used is made of two identical coils, characterized by an inner radius of 1.15 mm, an outer radius of $r = 1.39$ mm, a number of turns of 90, a height of 1.2 mm, and a lift-off of 0.1 mm. They operate in a T/R mode and are separated by a distance of $d = 6$ mm. The ratio $R_r/d = \frac{r}{d}$ in this case equals to $R_r/d = 0.23$. The frequency of the driving current in the transmitting coil is 1 MHz. The corresponding skin depth is of 0.5 mm.



Motion of the probe



Motion of the probe

Fig. 1. Probe in "T/R 1" orientation

Fig. 2. Probe in "T/R 2" orientation

The probe is used in two orientations: in the first one, denoted by "T/R 1", the axis fixed by the center of the two coils is parallel to the length of the flaw, whereas in the second orientation, called "T/R 2", the axis is orthogonal to the length of the flaw, as represented in Fig.1 and Fig.2. Four curves, representing signals yielded by VIM, HybM, SIM and then the experimental data, are plotted in each figure. The number of cells assuming pulse testing functions for the approximation of $\mathbf{P}(\mathbf{r})$ in the Method-of-Moments scheme is given in parentheses for VIM and HybM, under the

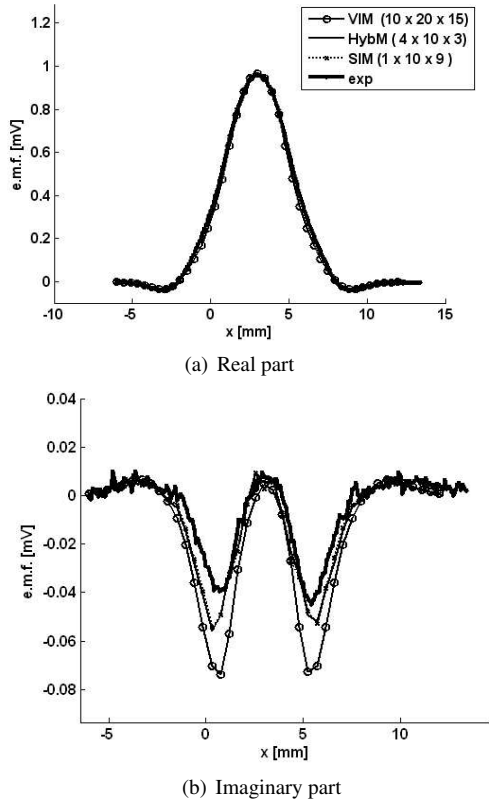


Fig. 3. Probe response for "N2" (60%), "T/R 1" orientation

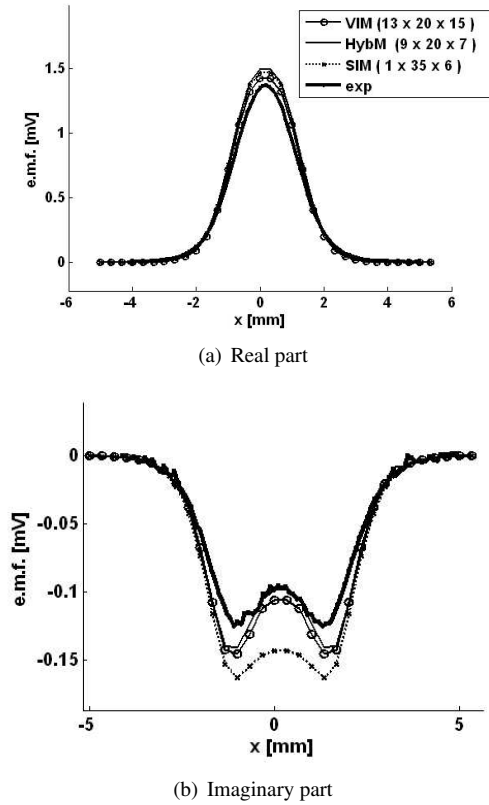


Fig. 4. Probe response for "N1" (80%), "T/R 1" orientation

	VIM	HybM	SIM
N1 / "TR1"			
Difference with exp	5%	9%	11%
Computational Times	15'	5'	1'40
N1 / "TR2"			
Difference with exp	16%	4%	17%
Computational Times	9'	2'	1'15

TABLE I. INDICATIONS ON THE RESULTS

format $(n_x \times n_y \times n_z)$. The number of global approximating functions is given in the same manner for SIM. Signals are normalized using their own maximum values, obtained on "N2" notch (60%) in the "T/R 1" orientation. Fig. 3(a) and 3(b) display respectively the real and imaginary parts of the normalized signals.

In Fig. 4(a) and 4(b) are plotted the real and imaginary parts of the signals obtained in the case of the "N1" notch (80%) in the "T/R 1" orientation. Differences on the maximum magnitude between the signal yielded by each model and experimental data, as well as the corresponding computational times on a standard PC (Pentium R, 3.20 GHz, RAM : 512 Mo) for a line scanning, are given in Table I. For a complete cartography involving e.g. 18 lines and 31 rows, these times become 5 hours, 4 minutes and 2 minutes for VIM, HybM and SIM, respectively. We conclude to a good agreement, concerning shapes and magnitudes of the signals, as well as low computational times for SIM and HybM.

Fig. 5(a) and 5(b) display respectively the real and imaginary parts of the signals yielded in considering the "N1" notch (80%) in the "T/R 2" orientation. It is noteworthy that the magnitude of the signals are more than 10 times smaller than those obtained in the previous configuration, and this is the reason why actual tests are usually not performed with

a probe in this orientation. The difference on the maximum of the magnitude between the results yielded by each model and experimental data, as well as computational times, are given in Table I, too. Moreover, Fig. 5(b) reveals that the imaginary part of SIM signal largely differs from experiment. These results illustrate the interest of the correction brought by HybM.

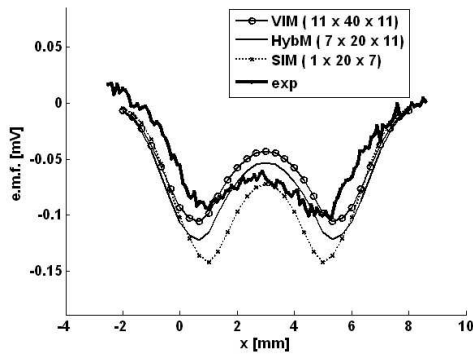
To study more accurately this shape difference, we carried out numerical tests on a configuration for which VIM results have already been validated, as presented in the next paragraph.

B. Numerical study on a second arrangement

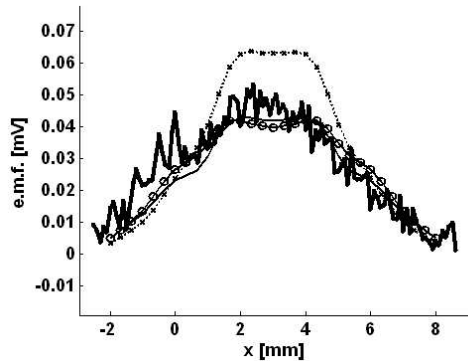
We now consider a surface breaking flaw with a depth of 0.61 mm, a length of 4 mm, and a thickness of 0.11 mm, affecting a slab made of Inconel 600 and again 1.55 mm thick. The operating probe is made of two identical coils characterized by an inner radius of 1 mm, an outer radius of $r = 1.6$ mm, a height of 2 mm, and a number of turns of 328, separated by $d = 4.2$ mm. The operating frequency is of 500 kHz, the skin depth is of 0.67 mm. The ratio R_r/d amounts this time to 0.38. We focus on the "T/R 2" orientation. The results yielded by the three models are given in Fig. 6(a). We notice a striking shape difference between SIM and the two other models, which we did not observe previously with a ratio of $R_r/d = 0.23$.

While increasing regularly the distance between the two coils, from $d = 4$ to $d = 8$ mm, we observe a gradual transformation of the signal yielded by SIM. For a choice of $d = 7$ mm, corresponding to $R_r/d = 0.23$, the big shape difference does not appear anymore as shown in Fig. 6(b). Some other parameters, e.g. the length of the flaw, may intervene in these shape differences.

These numerical experiments reveal some other impact on



(a) Real part



(b) Imaginary part

Fig. 5. Probe response for "N1" (80%), "TR 2" orientation

the strong restrictions made by the idealization of the planar flaw by the ideal crack, namely described by equation (2). Moreover, for all of cases tested, HybM provides results closer to VIM than SIM does, making it more reliable.

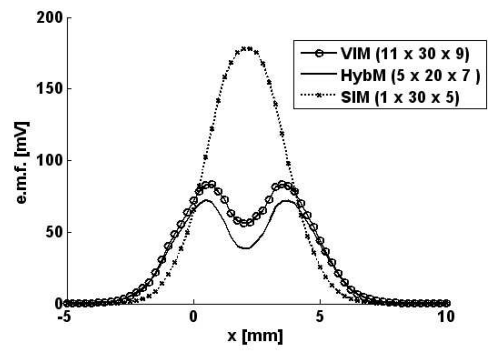
C. Conclusion

We have developed HybM based on a combination of VIM and SIM. HybM computations are carried out using the scalar density $p(\mathbf{r}_s)$, fast yielded by SIM, and then the whole primary field and the actual volume of the flaw are taken into account, ensuring more accuracy than SIM. Nevertheless, as it does not require so many computations as VIM, it is not computationally costly in contrast with VIM.

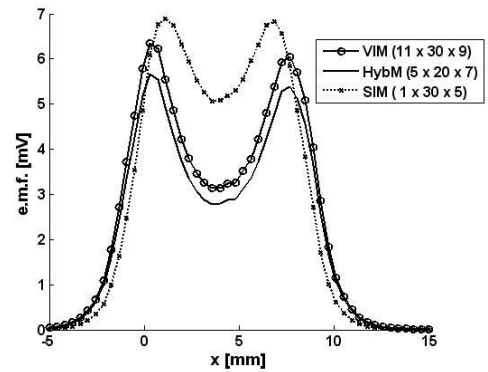
The three models have been compared using validation results with a T/R probe in two different orientations, showing a good agreement between the three models as well as low computational times for SIM and HybM. To sum up, it appears that HybM is efficient regarding the accuracy of the results, the computational time and memory load, and its reliability in many NDT configurations. One possible extension of this work is to tackle NDT configurations involving multiple cracks.

REFERENCES

- [1] J.R Bowler, "Eddy-current interaction with an ideal crack. Part I. The forward problem," *J. Appl. Phys.*, Vol. 75, no 12, pp. 8128-8137, 1994.
- [2] P. Beltrame and N. Burais, "Computing methods of hypersingular integral applied to eddy-current testing," *IEEE Trans. Magn.*, Vol. 38, no. 2, pp. 1269-1272, 2002.
- [3] P. Beltrame and N. Burais, "Application of regularization method of quasi-singular integrals to compute eddy-current



(a) For $d = 4.2$ mm .



(b) For $d = 7$ mm

Fig. 6. (a) Magnitude of the *e.m.f.* yielded by VIM, HybM and SIM, for two different values of d between the coils.

- distribution near cracks," *Int. J. Comp. Math. Engng*, Vol. 21, no. 4, pp. 519-533, 2002.
- [4] J. Pávó and K. Miya, "Reconstruction of crack shape by optimization using eddy current field measurement," *IEEE Trans. Magn.*, Vol. 30, no. 5, pp. 3407-3410, 1994.
- [5] J. R. Bowler, Y. Yoshida, and N. Harfield, "Vector potential boundary integral evaluation of eddy current interaction with a crack," *IEEE Trans. Magn.*, Vol. 33, no. 5, pp. 4287-4294, 1997.
- [6] J. Pávó, D. Prémel, and D. Lesselier, "Application of volumetric and surface defect models for the analysis of eddy current non-destructive testing problems," *Proc. URSI International Symposium on Electromagnetic Theory*, pp. 400-402, 2004.
- [7] Y. Deng, X. Liu, Z. Zeng, L. Udpa, W. Shih, and G. Fitzpatrick, "Numerical studies of magneto-optic imaging for probability of detection calculations," *Electromagnetic Non-destructive Evaluation*, vol. IX, L. Udpa and N. Bowler (eds), IOS Press, pp. 33-40, 2005.
- [8] F. Buvat, G. Pichenot, D. Prémel, D. Lesselier, M. Lambert, H. Voillaume, and J.P. Choffy, "Eddy-current modelling of ferrite-cored probes," *Review of Quantitative Non-destructive Evaluation (QNDE 2004)*, Vol. 23A, pp. 463-470, AIP Conference proceedings, 2005.
- [9] D. Prémel, G. Pichenot and T. Sollier, "Development of a 3D electromagnetic model for eddy current tubing inspection," *Int. J. Appl. Electromagn. Mechan.*, **19**, pp. 521-525, 2004.
- [10] W.C. Chew, "Waves and Fields in Inhomogeneous Media," 2nd edition, *IEEE Press*, Piscataway, 1995.
- [11] J. Pávó and D. Lesselier, "Calculation of eddy current testing probe signal with global approximation," *IEEE Trans. Magn.*, Vol. 42, no. 4, pp. 1419-1422, 2006.
- [12] B.A. Auld and J.C. Moulder, "Review of advances in quantitative eddy current non Destructive evaluation," *J. Nondestruct. Eval.*, Vol. 18, no 1, pp. 3-10, 1999.
- [13] CIVA: Simulation Software for Non Destructive Testing, www-civa.cea.fr.